J|A|C|S
ARTICLES
Published on Web 06/29/2006

Sharing Orbitals: Ultrafast Excited State Deactivations with Different Outcomes in Bucky Ferrocenes and Ruthenocenes

Dirk M. Guldi,*[,†] G. M. Aminur Rahman,[†] Renata Marczak,[†] Yutaka Matsuo,[‡] Masahiro Yamanaka,[§] and Eiichi Nakamura*[,‡,§]

Contribution from the Universität Erlangen, Institute for Physical and Theoretical Chemistry, 91058 Erlangen, Germany, Nakamura Functional Carbon Cluster Project, ERATO, Japan Science and Technology Agency, and Department of Chemistry, The University of Tokyo, Hongo, Bunkyo-ku, Tokyo 113-0033, Japan

Received February 16, 2006; E-mail: dirk.guldi@chemie.uni-erlangen.de; nakamura@chem.s.u-tokyo.ac.jp

Abstract: We report on the singlet ground and singlet/triplet excited-state features of a series of bucky ferrocenes, bucky ruthenocenes, and respective reference compounds. In the bucky ferrocene conjugates, intimate contacts between the fullerenes and ferrocenes result in appreciable ground-state interactions—suggesting a substantial shift of charge density from the electron donor (i.e., ferrocene) to the electron acceptor (i.e., fullerene). In contrast, no prominent charge-transfer features were observed for the bucky ruthenocene conjugates. An arsenal of experimental techniques, ranging from fluorescence (i.e., steady state and time-resolved) and pump probe experiments (i.e., femtosecond and nanoseconds) to pulse radiolysis, were employed to examine excited-state interactions. In the excited states, bucky ferrocene conjugates are dominated by rapid charge separation reactions (0.8 ± 0.1 ps) to yield metastable radical ion pairs. The radical ion pair lifetimes vary between 27 and 39 ps. No charge separation was, however, found in the corresponding bucky ruthenocence. Instead, an intrinsically faster excited-state deactivation ($\sim$ 200 ps) evolves from the heavier ruthenium center—relative to iron. This effect is further augmented by the unfavorably shifted oxidation potential in ruthenocene of about 0.61 V, which in ruthenocene ($-\Delta G_{ET} = -0.26$ eV), in contrast to ferrocene ($-\Delta G_{ET} = 0.35$ eV), renders charge separation thermodynamically unfeasible.

Introduction

Three-dimensional fullerenes are made of alternating hexagons (i.e., electron rich) and pentagons (i.e., electron deficient) with diameters starting at 7.8 Å for C_{60}.[1] Their extraordinary electron acceptor properties have resulted in noteworthy advances in the areas of light-induced electron-transfer chemistry and solar-energy conversion.[2] It is mainly the small reorganization energy, which fullerenes exhibit in electron-transfer reactions, that is accountable for a noteworthy breakthrough.[3] In particular, ultrafast charge separation together with very slow charge recombination features lead to unprecedented long-lived radical ion pair states formed in high quantum yields.[4]

In the general context of electron donor-acceptor interactions, ferrocene represented one of the first electron donors that was integrated—together with an electron-accepting fullerene—into a series of novel conjugates.[5] Later, this initial work was complemented by investigations that assisted in elucidating a series of fundamental aspects. In this context, variable compositions of a ferrocene linked to fullerenes (yielding artificial light-harvesting antenna and reaction center mimics) have been utilized to fine-tune the electronic coupling, orientation, and separation between donor and acceptor sites and the total reorganization energy.[2] All these parameters bear great impact on the rate, yield, and lifetime of the energetic charge separated

[†] Universität Erlangen.
[‡] Nakamura Functional Carbon Cluster Project, ERATO.
[§] The University of Tokyo.

(1) (a) Kroto, H. W. *Nature* **1987**, *329*, 529. (b) Krätschmer, W.; Lamb, L. D.; Fostiropulos, K.; Huffmann, D. R. *Nature*, **1990**, *347*, 354. (c) Haddon, R. C.; Brus, L. E.; Raghavachari, K. *Chem. Phys. Lett*. **1986**, *131*, 165. (d) Morton, J. R.; Negri; F.; Preston, K. F. *Acc. Chem. Res*. **1998**, *31*, 63. (e) Rosseinsky, M. J. *J. Mater. Chem*. **1995**, *5*, 1497. (f) Weaver, J. H. *Acc. Chem. Res*. **1992**, *25*, 143.

(2) (a) Imahori, H.; Sakata, Y. *Adv. Mater*. **1997**, *9*, 537. (b) Prato, M. *J. Mater. Chem.* **1997**, *7*, 1097. (c) Martin, N.; Sanchez, L.; Illescas, B.; Perez, I. *Chem. Rev*. **1998**, *98*, 2527. (d) Imahori, H.; Sakata, Y. *Eur. J. Org. Chem.* **1999**, 2445. (e) Diederich, F.; Gomez-Lopez, M. *Chem. Soc. Rev.* **1999**, *28*, 263. (f) Guldi, D. M. *Chem. Commun*. **2000**, 321. (g) Reed C. A.; Bolskar, R. D. *Chem. Rev*. **2000**, *100*, 1075. (h) Gust, D.; Moore, T. A.; Moore, A. L. *J. Photochem. Photobiol., B* **2000**, *58*, 63. (i) Gust, D.; Moore, T. A.; Moore, A. L. *Acc. Chem. Res*. **2001**, *34*, 40. (j) Guldi, D. M.; Martin, N. *J. Mater. Chem.* **2002**, *12*, 1978. (k) Guldi, D. M. *Chem. Soc. Rev.* **2002**, *31*, 22. (l) Imahori, H.; Mori, Y.; Matano, Y. *J. Photochem. Photobiol., C* **2003**, *4*, 51. (m) Nierengarten, J. F. *Top. Curr. Chem.* **2003**, *228*, 87. (n) Guldi, D. M. *Pure Appl. Chem.* **2003**, *75*, 1069. (o) El-Khouly, M. E.; Ito, O.; D'Souza, F. *J. Photochem. Photobiol., C* **2004**, *5*, 79. (p) Guldi, D. M.; Prato, M. *Chem. Commun.* **2004**, 2517. (q) Guldi, D. M. *J. Phys. Chem. B* **2005**, *109*, 11432.

(3) (a) Imahori, H.; Hagiwara, K.; Akiyama, T.; Aoki, M.; Taniguchi, S.; Okada, T.; Shirakawa, M.; Sakata, Y. *Chem. Phys. Lett*. **1996**, *263*, 545. (b) Guldi, D. M.; Asmus, K.-D. *J. Am. Chem. Soc*. **1997**, *119*, 5744. (c) Fukuzumi, S.; Ohkubo, K.; Imahori, H.; Guldi, D. M. *Chem. Eur. J.* **2003**, *9*, 1585. (d) Guldi, D. M. *Spectrum* **2003**, *16*, 8.

(4) (a) Imahori, H.; Guldi, D. M.; Tamaki, K.; Yoshida, Y.; Luo, C.; Sakata, Y.; Fukuzumi, S. *J. Am. Chem. Soc.* **2001**, *123*, 6617. (b) Guldi, D. M.; Imahori, H.; Tamaki, K.; Kashiwagi, Y.; Yamada, H.; Sakata, Y.; Fukuzumi, S. *J. Phys. Chem. A* **2004**, *108*, 541. (c) Imahori, H.; Sekiguchi, Y.; Kashiwagi, Y.; Sato, T.; Araki, Y.; Ito, O.; Yamada, H.; Fukuzumi, S. *Chem. Eur. J.* **2004**, *10*, 3184.

(5) Guldi, D. M.; Maggini, M.; Scorrano, G.; Prato, M. *J. Am. Chem. Soc.* **1997**, *119*, 974.

 10.1021/ja061120v CCC: $33.50

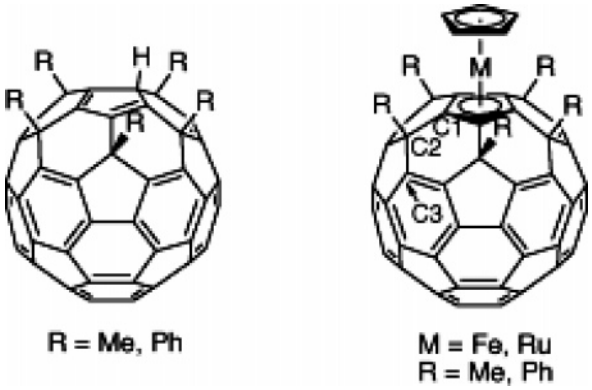

Figure 1. Penta(organo)hydro[60]fullerenes (i.e., $C_{60}Me_5H$ and $C_{60}Ph_5H$) and bucky metallocenes (i.e., iron: $Fe(C_{60}Me_5)Cp$, $Fe(C_{60}Ph_5)Cp$; ruthenium: $Ru(C_{60}Me_5)Cp$, $Ru(C_{60}Ph_5)Cp$). The numbering defines the dissecting plane used in Figure 2.

states. For example, ferrocene was employed to signal the electron-transfer deactivation in fulleropyrrolidine versus fulleropyrrolidinium salts, revealing that the corresponding zwitterionic species accelerated charge separation and decelerated charge recombination dynamics.[6] Moreover, electron-donating ferrocenes, owing to their ease of oxidation, were frequently used as terminal building blocks in electron-transfer relay systems, namely, linear triads, tetrads, pentads.[4,7] In these conjugates, vectorial and directed multistep electron-transfer steps yield, due to enhanced spatial donor-acceptor separation, long-lived (i.e., seconds) radical ion pair states. Quite different is the work that shows the versatility of ferrocene and fullerene for the design of thermotropic liquid-crystalline materials, bearing cholesterol as a liquid-crystalline promoter.[8] More precisely, the electrochemical properties of the ferrocene−ferrocenium system were exploited to design redox-active metallomesogens.

One aspect that only finds sporadic consideration is to reduce the spatial separation between the electron-donating ferrocene and the fullerene core. One of the few examples is the case of an azafullerene-ferrocene conjugate, where the two electroactive groups are connected by only a single σ-bond.[9] In fact, strong electronic couplings cause an instantaneous deactivation of the photoexcited azafullerene. An ultimately short connection is achieved in "bucky ferrocenes" (Figure 1),[10] where ferrocene and fullerene share one pentagon and hence are fused together. Electrochemical data suggested that the ferrocene dπ-system and fullerene 50π-systems are homoconjugated within the interior of the fullerene core skeleton (endohedral homoconjugation).[11] Ruthenium congeners have also been reported.[12] Herein, we report the photophysical properties and photoinduced charge-separation processes with bucky ferrocenes and bucky ruthenocenes, $M(\eta^5\text{-}C_{60}R_5)(\eta^5\text{-}C_5H_5)$ (M = Fe and Ru; R = Me and Ph).

Results and Discussion

To obtain concrete ideas about the endohedral interaction between the ferrocene and the fullerene orbitals, quantum mechanical calculations (see for details the figure caption of Figure 2) were carried out for $Fe(\eta^5\text{-}C_{60}Me_5)(\eta^5\text{-}C_5H_5)$. Since the large size of the molecule does not allow full structural optimization of the molecule, the coordinates of the iron and the carbon atoms were fixed at the C_{5v} symmetric average of the experimental crystal structure, while the position of the hydrogen atoms were optimized. The orbital pictures in Figure 2 illustrate a fully extended d$-\pi$ conjugation system involving iron 3d and carbon π- and σ-orbitals. The in-phase interaction between the ferrocene and the bottom C_{50} moieties, indicated by the green circle in the HOMO-11 orbital (E_1, −6.88 eV, Figure 2b), supports the presence of weak homoconjugation.

At first glance the absorption spectra of all investigated samples (regardless of the electron donors) show the typical fullerene patterns, namely, strong absorptions in the UV (i.e., 350 and 395 nm) and weaker transitions in the visible (i.e., 470 nm). However, the intimate contacts between the electron acceptor (i.e., fullerene) and the electron donors (i.e., ferrocene or ruthenoecene), in the form of small orbital overlaps, lead to significant electronic perturbations. Such interactions are even appreciable in the ground-state configuration and suggest a measurable shift of charge density from the electron donor (i.e., ferrocene) to the electron acceptor (i.e., fullerene). As demonstrated in Figure 3 the absorption spectra fail to be linear superimpositions of the individual component spectra. Close inspection of the difference spectra between $C_{60}Ph_5H$ and $Fe(C_{60}Ph_5)Cp$ or $C_{60}Me_5H$ and $Fe(C_{60}Me_5)Cp$ unravels, for example, fairly strong charge-transfer features in the visible region. The new features essentially resemble those detected in previously studied fullerene-ferrocene conjugates.[5] In toluene, the following parameters are derived for $Fe(C_{60}Ph_5)Cp$ and $Fe(C_{60}Me_5)Cp$: $\epsilon_{max} = 565 \pm 25\ M^{-1}\ cm^{-1}$; $\nu_{max} = 17850 \pm 500\ cm^{-1}$, $\Delta\nu_{1/2} = 1726 \pm 200\ cm^{-1}$.

The charge transfer is primarily a consequence of the strong electronic coupling (V) between electron donor and electron acceptor, which determined via

$$V = \frac{2.06 \times 10^{-2}\sqrt{\epsilon_{max}\nu_{max}\Delta\nu_{1/2}}}{R_{cc}} \qquad (1)$$

are $485 \pm 5\ cm^{-1}$ ($Fe(C_{60}Ph_5)Cp$) and $460 \pm 5\ cm^{-1}$ ($Fe(C_{60}Me_5)Cp$) at center-to-center distances (R_{cc}) of 5.5 Å.

Relative to those of previously studied fullerene−ferrocene conjugates, such high V values represent an amplification of at

(6) (a) Guldi, D. M.; Luo, C.; Da Ros, T.; Bosi, S.; Prato, M. *Chem. Commun.* **2002**, 2320. (b) Guldi, D. M.; Luo, C.; Koktysh, D.; Kotov, N. A.; Da Ros, T.; Bosi, S.; Prato, M. *Nano Lett.* **2002**, *2*, 775. (c) Guldi, D. M.; Luo, C.; Kotov, N. A.; Da Ros, T.; Bosi, S.; Prato, M. *J. Phys. Chem. B* **2003**, *107*, 7293.
(7) (a) Luo, C.; Guldi, D. M.; Imahori, H.; Tamaki, K.; Sakata, Y. *J. Am. Chem. Soc.* **2000**, *122*, 6535. (b) Imahori, H.; Yamada, H.; Guldi, D. M.; Endo, Y.; Shimomura, A.; Kundu, S.; Yamada, K.; Okada, T.; Sakata, Y.; Fukuzumi, S. *Angew. Chem., Int. Ed.* **2002**, *41*, 2344.
(8) (a) Deschenaux, R.; Even, M.; Guillon, D. *Chem. Commun.* **1998**, 537. (b) Chuard, T.; Deschenaux, R. *Chimia* **2001,** *55*, 139. (c) Even, M.; Heinrich, B.; Guillon, D.; Guldi, D. M.; Prato, M.; Deschenaux, R. *Chem. Eur. J.* **2001**, *7*, 2595. (d) Campidelli, S.; Vazquez, E.; Milic, D.; Prato, M.; Barbera, J.; Guldi, D. M.; Marcaccio, M.; Paolucci, D.; Paolucci, F.; Deschenaux, R. *J. Mater. Chem.* **2004**, 1266.
(9) Hauke, F.; Hirsch, A.; Liu, S.-G.; Echegoyen, L.; Swartz, A.; Luo, C.; Guldi, D. M. *ChemPhysChem* **2002**, *3*, 195.
(10) (a) Sawamura, M.; Kuninobu, Y.; Toganoh, M.; Matsuo, Y.; Yamanaka, M.; Nakamura, E. *J. Am. Chem. Soc.* **2002**, *124*, 9354. (b) Toganoh, M.; Matsuo, Y.; Nakamura, E. *J. Am. Chem. Soc.* **2003**, *125*, 13974. (c) Nakamura, E. *J. Organomet. Chem.* **2004**, *689*, 4630. (d) Herber, R. H.; Nowik, I.; Matsuo, Y.; Toganoh, M.; Kuninobu, Y.; Nakamura, E. *Inorg. Chem.* **2005**, *44*, 5629. (e) Matsuo, Y.; Isobe, H.; Tanaka, T.; Murata, Y.; Murata, M.; Komatsu, K.; Nakamura, E. *J. Am. Chem. Soc.* **2005**, *127*, 17148.
(11) (a) Sawamura, M.; Iikura, H.; Nakamura, E. *J. Am. Chem. Soc.* **1996**, *118*, 12850. (b) Iikura, H.; Mori, S.; Sawamura, M.; Nakamura, E. *J. Org. Chem.* **1997**, *62*, 7912.
(12) Matsuo, Y.; Kuninobu, Y.; Ito, S.; Nakamura, E. *Chem. Lett.* **2004**, *33*, 68.

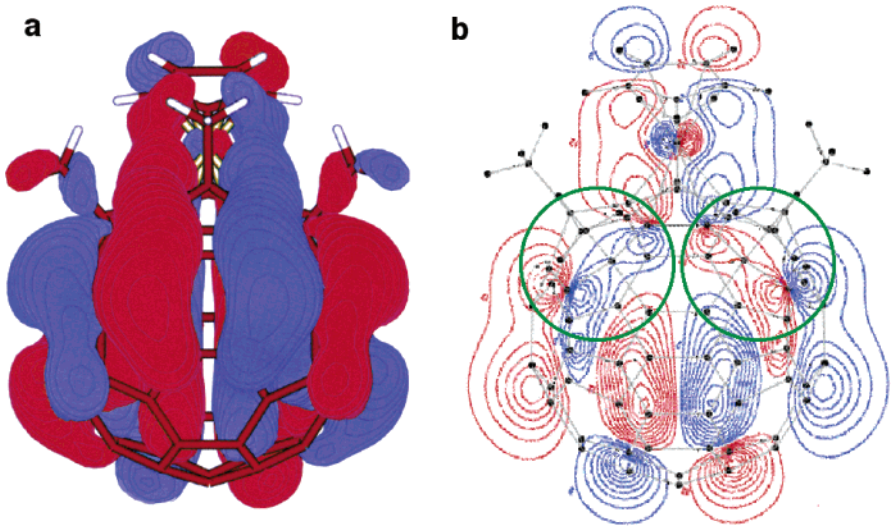

Figure 2. Molecular orbital of Fe(η^5-$C_{60}Me_5$)(η^5-C_5H_5) obtained by DFT calculations for the geometry of the crystal structure (C_{5v} symmetry) that shows a fully extended d−π conjugation system involving iron 3d and carbon orbitals. (a) 3D Snapshot. (b) Contour plot in the C1−C2−C3 plane defined in Figure 1 (intervals of 0.005 e·Å^{-3}) of the HOMO−11 orbital (E_1, −6.88 eV). Note the in-phase interaction between the ferrocene and the bottom C_{50} moieties (green circle). The corresponding out-of-phase interaction of the two parts is found as a higher-energy orbital (HOMO−8, E_1, −6.54 eV, not shown).

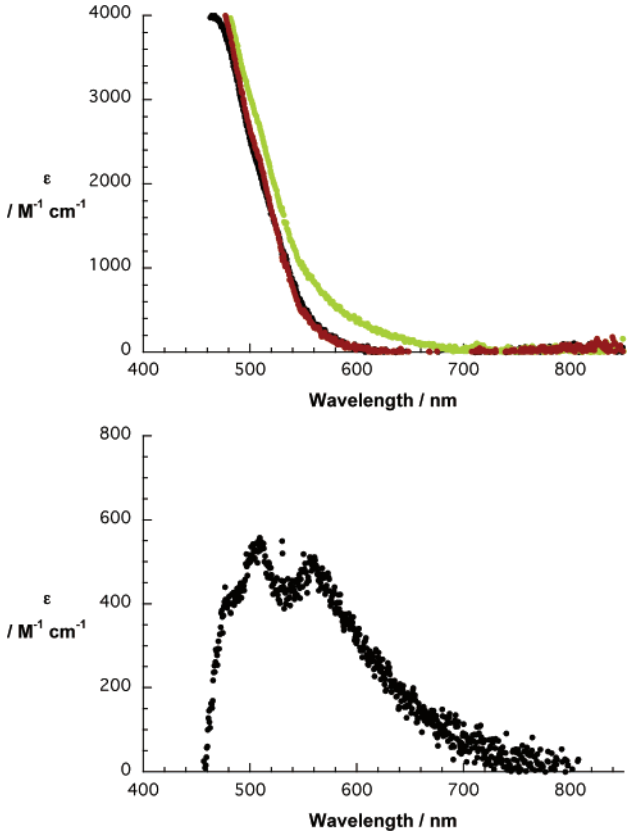

Figure 3. (Top) Absorption spectra of $C_{60}Ph_5H$ (black), Fe($C_{60}Ph_5$)Cp (green), and Ru($C_{60}Ph_5$)Cp (red) in toluene. (Bottom) Charge-transfer band of Fe($C_{60}Ph_5$)Cp in toluene.

least 1 order of magnitude.[5] For example, in a directly C−C linked C_{59}N-ferrocene conjugate we found a moderate coupling of 58 cm^{-1}.[9] No orbital overlap is realized, however, in this particular C_{59}N-ferrocene conjugate. Only topologically enforced π−π stacks of fullerenes and porphyrins have coupling elements that are comparable to those of the currently tested Fe($C_{60}Ph_5$)Cp and Fe($C_{60}Me_5$)Cp conjugates—although to a lesser extent.[13]

Important is the fact that no detectable charge-transfer features were seen for the Ru($C_{60}Ph_5$)Cp and Ru($C_{60}Me_5$)Cp conjugates, whose absorptions are best described as the linear sum of Ru(Cp)$_2$ and $C_{60}Ph_5H$ or $C_{60}Me_5H$, respectively.

Quantitative analysis of the redox potentials (i.e., acceptor reduction and donor oxidation) in the donor-acceptor conjugates points essentially to the same conclusion. For bucky ferrocene, the fullerene reduction in $C_{60}Me_5H$ and Fe($C_{60}Me_5$)Cp and the ferrocene oxidation in Fe(Cp)$_2$ and Fe($C_{60}Me_5$)Cp are affected by a 0.01 V negative shift and a 0.22 V positive shift, respectively. The lower impact on the fullerene reduction is rationalized on the basis of the small reorganization of fullerenes in electron transfer (especially the internal reorganization) which has been shown at numerous occasions to diminish the fullerene's susceptibility for measurable electronic changes.[13] For bucky ruthenocene, on the other hand, the fullerene reduction shifts positively by 0.05 V, while the ruthenocene oxidation is not noticeably altered.

In view of the ground-state changes we employed fluorescence spectroscopic tools—steady-state and time-resolved fluorescence—to probe excited-state deactivation. Both fullerenes that lack the electron-donating ferrocene or ruthenocene, that is, $C_{60}Me_5H$ and $C_{60}Ph_5H$, emerged hereby as important reference systems.[10−12] Relative to the widely studied fulleropyrrolidines, a number of significant differences should be brought together (see Figure 3 and Table 1). First, the fluorescence quantum yields are increased (i.e., (2.2 ± 0.1) × 10^{-3} versus (6.0 ± 0.1) × 10^{-4}). Second, the fluorescence maxima are blue-shifted (i.e., 615 nm versus 720 nm). Third, the spectra are broadened. Finally, methyl or phenyl substituents impact the fluorescence quantum yields with values of (2.2 ± 0.1) × 10^{-3} and (1.5 ± 0.1) × 10^{-3}, respectively. Overall, the features are somewhat similar to those reported for highly

(13) (a) Guldi, D. M.; Scheloske, M.; Dietel, E.; Hirsch, A.; Troisi, A.; Zerbetto, F.; Prato, M. *Chem. Eur. J.* **2003**, *9*, 4968. (b) Chukharev, V.; Tkachenko, N. V.; Efimov, A.; Guldi, D. M.; Hirsch, A.; Scheloske, M.; Lemmetyinen, H. *J. Phys. Chem. B* **2004**, *108*, 16377. (c) Armaroli, N.; Marconi, G.; Echegoyen, L.; Bourgeois, J.-P.; Diederich, F. *Chem. Eur. J.* **2000**, *6*, 1629.

Table 1. Photophysical Properties of Bucky Ferrocene and Ruthenocene

	$C_{60}Me_5H$	$C_{60}Ph_5H$	$Fe(C_{60}Me_5)Cp$	$Fe(C_{60}Ph_5)Cp$	$Ru(C_{60}Me_5)Cp$	$Ru(C_{60}Ph_5)Cp$
fluorescence (Φ) toluene	2.2×10^{-3}	1.5×10^{-3}	2.4×10^{-5}	3.3×10^{-5}	2.6×10^{-4}	2.7×10^{-4}
fluorescence (Φ) thf	2.2×10^{-3}	1.4×10^{-3}	1.6×10^{-5}	2.6×10^{-5}	2.9×10^{-4}	1.8×10^{-4}
fluorescence (Φ) bzcn	2.2×10^{-3}	1.4×10^{-3}	1.4×10^{-5}	2.3×10^{-5}	3.2×10^{-4}	2.3×10^{-4}
fluorescence (τ) toluene	710 ps	650 ps			275 ps	220 ps
fluorescence (τ) thf	690 ps	585 ps			290 ps	170 ps
fluorescence (τ) bzcn	650 ps	530 ps			280 ps	180 ps
singlet (τ) toluene	705 ps	615 ps	0.8 ps	0.9 ps	190 ps	210 ps
singlet (τ) thf	650 ps	550 ps	0.7 ps	0.7 ps	not determined	not determined
radical ion pair (τ) toluene			35 ps	39 ps		
radical ion pair (τ) thf			28 ps	27 ps		
triplet bzcn	95%	100%			96%	92%

symmetric fullerene adducts, such as the recently studied T_h-hexakis adducts.[14]

Figure 4 illustrates that when comparing the fluorescence of the ferrocene containing conjugates with that of the reference systems, a significant quenching (i.e., quantum yields of around 10^{-5}) of the fullerene-centered fluorescence is noted. Such quenching prompts ultafast singlet excited-state deactivations with underlying rate constants that exceed a limit of 10^{11} s^{-1}. This ultrafast deactivation is in line with (i) the close spatial donor-acceptor separation, (ii) the strong electronic coupling elements, and (iii) the largely affected oxidation potential of $Fe(Cp)_2$. In sharp contrast, the ruthenocene-containing conjugates give rise to a much weaker fluorescence quenching (i.e., quantum yields of around 10^{-4}). Another fundamental difference between the $Fe(C_{60}Ph_5)Cp$/$Fe(C_{60}Me_5)Cp$ and $Ru(C_{60}Ph_5)Cp$/$Ru(C_{60}Me_5)Cp$ conjugates is seen when inspecting the following solvent series: toluene, THF, and benzonitrile. While in the ferrocene cases the quantum yields drop continuously when going from the nonpolar to the polar media, the analogous variation in the ruthenocene is virtually insignificant.

The aforementioned trends are also reflected in the time-resolved fluorescence decay measurements, see Table 1. For example, fluorescence lifetimes of 680 ± 30 ps and 280 ± 10 ps are seen for $C_{60}Me_5H$ and $Ru(C_{60}Me_5)Cp$ (see Figure S1). $Fe(C_{60}Ph_5)Cp$ and $Fe(C_{60}Me_5)Cp$, on the other hand, fail to generate any detectable fluorescence that exceeds the instrumental time limit of our apparatus. Consequently, we must assume that the fluorescence deactivation in the latter cases is significantly faster than 100 ps (i.e., $\gg 10^{10}$ s^{-1}).

Thermodynamic evaluations of the reaction pathways help to shed light onto the different photoreactivity. The fluorescence maxima are used to estimate the singlet excited-state energy of all the fullerene derivatives: 2.02 eV. The energy of the radical ion pairs were—as the sum of the oxidation and reduction potentials—1.67 and 2.28 eV for the ferrocene and ruthenocene derivatives, respectively. Our consideration supports, however, only an exothermic ($-\Delta G_{ET} = 0.35$ eV) charge-separation scenario that commences with the photoexcited fullerene in the ferrocene conjugates. Considering the energetic positioning of the charge-transfer bands in $Fe(C_{60}Me_5)Cp$ and $Fe(C_{60}Ph_5)Cp$ (2.2 eV) relative to the calculated energies of the radical ion pair states (1.67 eV) allows estimating moderate reorganization energies of ~0.6 eV. Consequently, charge separation and charge recombination reactions are located in the normal region or close to the thermodynamic maximum and deep in the inverted region of the Marcus parabola, respectively.[15] Conversely, for the ruthenocene conjugates the electron transfer is largely prohibited under ambient conditions on grounds of a substantially positive energy gap ($-\Delta G_{ET} = -0.26$ eV).

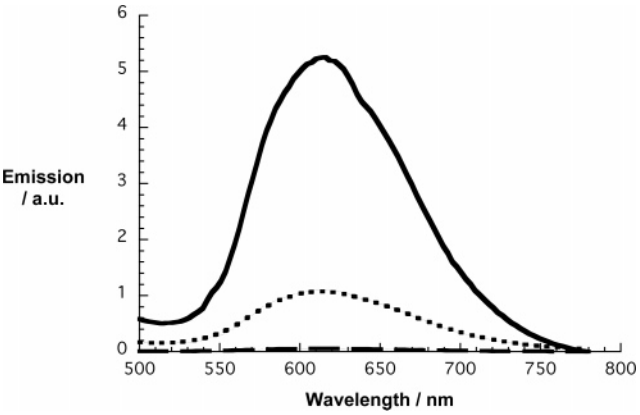

Figure 4. Room-temperature fluorescence spectra of $C_{60}Ph_5H$ (solid line), $Fe(C_{60}Ph_5)Cp$ (dashed line), and $Ru(C_{60}Ph_5)Cp$ (dotted line) in toluene recorded with solutions that exhibit optical absorptions of 0.2 at the 400-nm excitation wavelength.

Transduction of singlet excited-state energy (from the photoexcited fullerene to either ferrocene (2.46 eV)[16] or ruthenocene (2.65 eV)[16]) is also thermodynamically uphill and, thus, unlikely to play a meaningful role. Last, the energetically feasible singlet-triplet energy transfer with energy gaps of at least 1.0 eV should be considered. But spectroscopic evidence, vide infra, helps to eliminate such spin-forbidden energy-transfer processes in all systems (i.e., ferrocene and ruthenocene).

Next, transient absorption spectroscopy (i.e., 150-fs laser pulses at 387 nm and 8-ns laser pulses at 337 nm) was employed to confirm the ultrafast fullerene singlet excited-state deactivation and, in addition, to characterize the nature of the photoproducts. Again, $C_{60}Me_5H$ and $C_{60}Ph_5H$ were tested first as reference systems. Typical changes upon 150-fs laser excitation are depicted in Figure 5 for $C_{60}Ph_5H$. As the corresponding time-absorption profiles indicate, the singlet excited states are formed with rates of $\sim 1.2 \times 10^{12}$ s^{-1}, which is likely to involve internal deactivation starting from higher-lying excited states. Typical features of the singlet-singlet transitions are maxima at 585 and 760 nm. Multiwavelength analysis of the singlet decay, performed throughout the 400−800 nm range, reveals singlet lifetimes of 705 ± 10 ps (i.e., $C_{60}Me_5H$) and 615 ± 10 ps (i.e., $C_{60}Ph_5H$). These lifetimes are a quantitative match of the

(14) Guldi, D. M.; Swartz, A.; Luo, C.; Diekers, M.; Hirsch, A. *Chem. Eur. J.* **2002**, *8*, 979.

(15) Marcus, R. A. *Angew. Chem., Int. Ed. Engl.* **1993**, *32*, 1111.

(16) (a) Balzani, V.; Bolletta, F.; Scandola, F. *J. Am. Chem. Soc.* **1980**, *102*, 2152. (b) Riesen, H.; Krausz, E.; Luginbuehl, W.; Biner, M.; Guedel, H. U.; Ludl, A. *J. Chem. Phys.* **1992**, *96*, 4131.

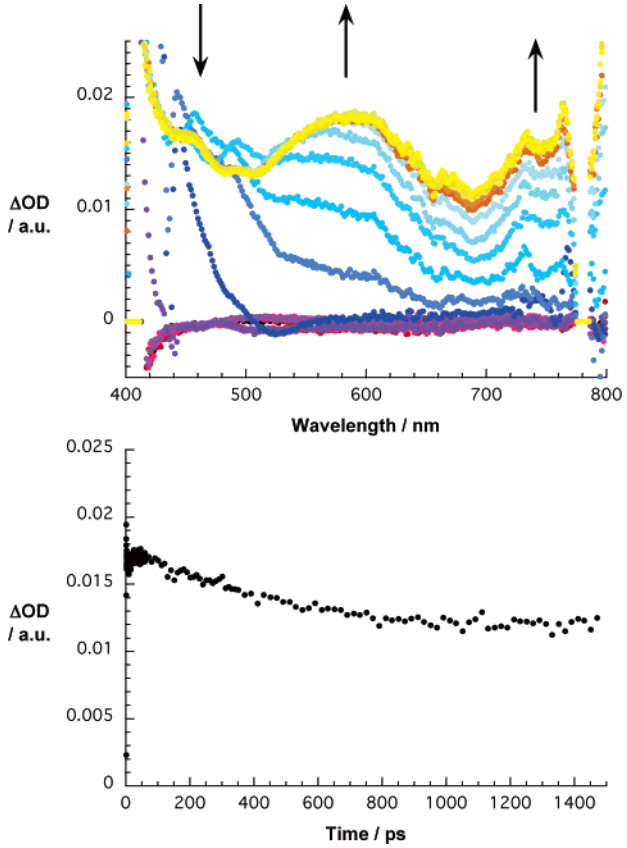

Figure 5. (Top) Differential absorption spectra (visible) obtained upon femtosecond flash photolysis (387 nm) of $C_{60}Ph_5H$ in nitrogen-saturated toluene with several time delays between 0 and 5 ps at room temperature. (Bottom) Time−absorption profiles of the spectra shown above at 450 nm, monitoring the decay of the fullerene singlet excited state.

fluorescence lifetimes. Implicit in the singlet decay is a spin-forbidden intersystem crossing that transforms the singlet excited states (~2.02 eV) into the energetically lower-lying triplet excited states (1.6 eV). The transient absorption spectra of the correspondingly formed triplet excited states show maxima at 660 nm—this was confirmed independently by recording the spectra at the conclusion of the femtosecond experiment time scale (not shown) and at the beginning of the nanosecond experiment time scale (Figure 6). In the absence of molecular oxygen the triplet lifetime of these fullerene references is about 14 ± 2 μs. When molecular oxygen is present, an efficient energy transfer with rate constants of $\sim 10^9$ M^{-1} s^{-1} (see Figure S2) takes place that leads to the quantitative generation of cytotoxic singlet oxygen.[17]

Both bucky ferrocenes (i.e., Fe($C_{60}Me_5$)Cp and Fe($C_{60}Ph_5$)-Cp) show differential absorption characteristics initially after laser excitation that resemble those seen in the reference systems, that is, the singlet-singlet attributes. This observation is vital, since it affirms the successful photoexcitation of the fullerene cores, despite the presence of the electron donor moieties and the strong, mutual coupling. For Fe($C_{60}Me_5$)Cp and Fe($C_{60}Ph_5$)-Cp the fullerene singlet excited-state deactivation is, however, nearly instantaneous. More precisely, singlet lifetimes of 0.9 ± 0.1 and 0.7 ± 0.1 ps were determined in toluene and THF, respectively. The product of this ultrafast decay bears no particular similarity with the fullerene triplet excited state, which

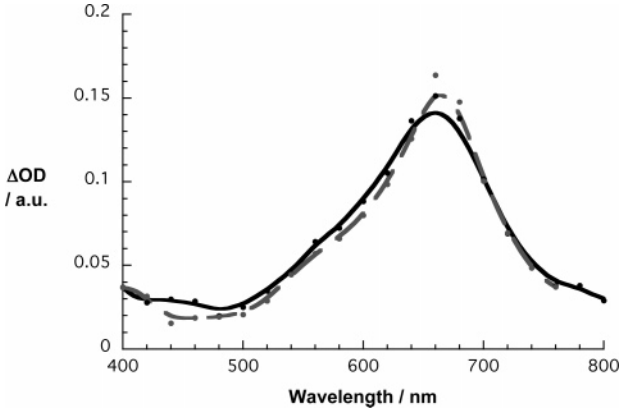

Figure 6. Differential absorption spectrum (visible) obtained upon nanosecond flash photolysis (337 nm) of $C_{60}Me_5H$ (solid line) and Ru(C_{60}-Me_5)Cp (dashed line) in nitrogen-saturated benzonitrile with a 100-ns time delay at room temperature.

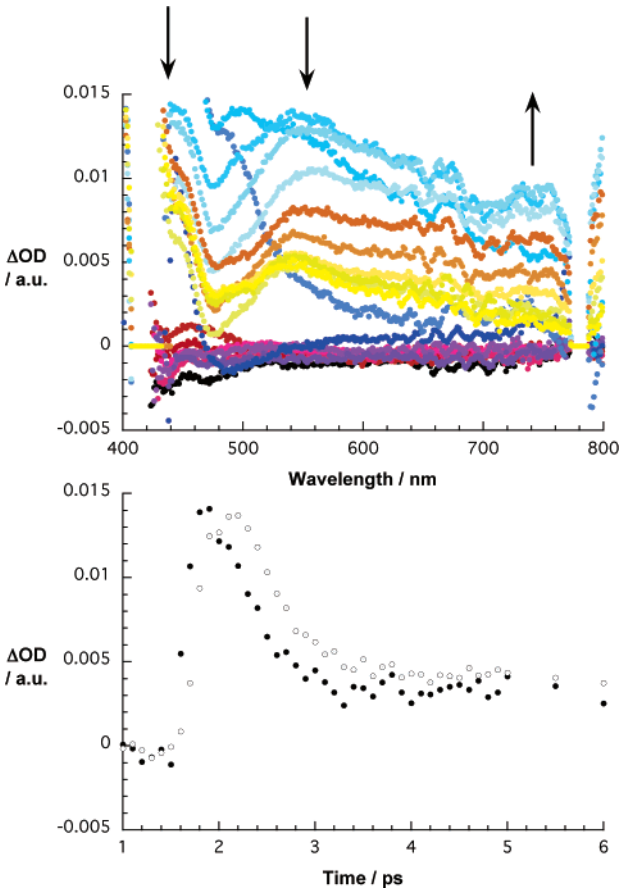

Figure 7. (Top) Differential absorption spectra (visible) obtained upon femtosecond flash photolysis (387 nm) of Fe($C_{60}Ph_5$)Cp in nitrogen-saturated toluene with several time delays between 0 and 5 ps at room temperature. (Bottom) Time−absorption profiles of the spectra shown above at 500 and 550 nm, monitoring the decay of the fullerene singlet excited state.

is formed in the absence of the electron donor (see above). Features of the new product, as shown in Figure 7, are transient maxima at <430 and 535 nm, plus a shoulder at 620 nm. We ascribe the earlier transitions to the one-electron reduced fullerene (vide infra). The latter, on the other hand, is assigned to the one-electron oxidized ferrocene, an assignment that is based on earlier work showing a weak absorption band at 625 nm for pulse radiolytically generated $[Fe(Cp)_2]^{\bullet+}$.[18] All radical

(17) Guldi, D. M.; Prato, M. *Acc. Chem. Res.* **2000**, *33*, 695.

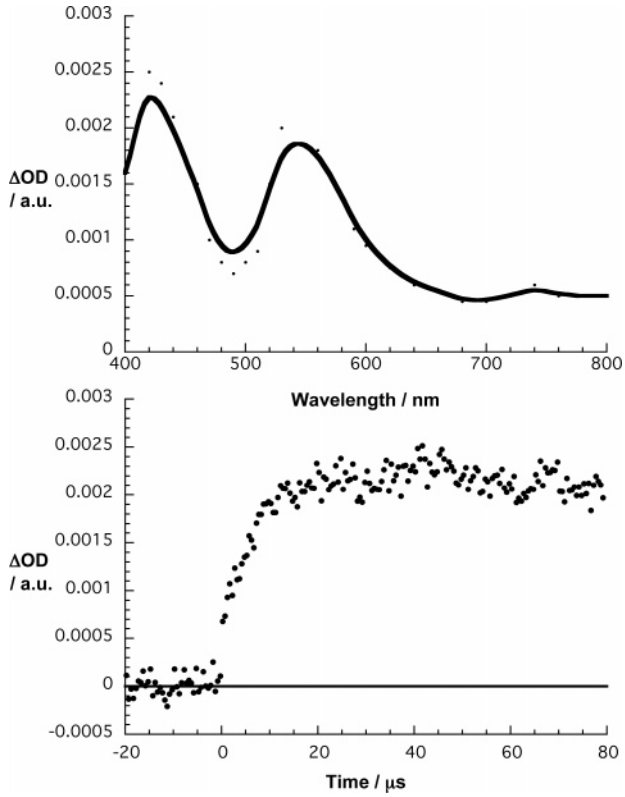

Figure 8. (Top) Differential absorption spectrum (visible) obtained upon pulse radiolytic reduction of $C_{60}Me_5H$ in a nitrogen-saturated solvent mixture of toluene, 2-propanol, and acetone (8:1:1 v/v). (Bottom) Time−absorption profiles of the spectrum shown above at 540 nm, monitoring the formation of the fullerene radical ion.

ion pair lifetimes, which are on the order of 30 ± 5 ps, reveal stabilization in the nonpolar environments (i.e., toluene versus THF). The trend of stabilization corroborates our earlier thermodynamic postulate, namely, that the strongly exothermic charge recombination dynamics are placed deep in the inverted region of the Marcus parabola.[15] In complementary nanosecond transient absorption measurements no photoproduct was recorded, which corroborates that charge recombination leads to the quantitative reconstitution of the singlet ground state.

To confirm our assignment of the spectral characteristics, additional pulse radiolytic reduction experiments with $C_{60}Me_5H$ and $C_{60}Ph_5H$ were deemed necessary in a solvent mixture containing toluene, 2-propanol, and acetone (see Experimental Section for details). In particular, in the absence of molecular oxygen strongly reducing $(CH_3)_2{}^{\bullet}COH$ and $(CH_3)_2{}^{\bullet}CO^-$ are formed, which have been shown to be sufficiently reactive to reduce C_{60}, higher fullerenes, and a number of fullerene derivatives.[19] The differential absorption spectrum following the conclusion of the radiolytic reduction of $C_{60}Me_5H$ is shown in Figure 8. A set of maxima (at 425 and 540 nm) appears under pseudo-first-order conditions. These characteristics are in excellent agreement with the features seen in the femtosecond experiments and support the following reaction pathway:

$$Fe(C_{60}R_5)Cp \xrightarrow{h\nu} Fe(^1{}^*C_{60}R_5)Cp \xrightarrow{CS} Fe^{\bullet+}(C_{60}{}^{\bullet-}R_5)Cp \xrightarrow{CR} Fe(C_{60}R_5)Cp \quad (2)$$

Immediately upon photoexciting $Ru(C_{60}Me_5)Cp$ and $Ru(C_{60}Ph_5)Cp$ the fullerene singlet excited-state attributes are also discernible. In line with the fluorescence experiments the singlet lifetimes (Figure S3) are shorter [with values of 190 ps ($Ru(C_{60}Me_5)Cp$) and 210 ps ($Ru(C_{60}Ph_5)Cp$)] than those in the fullerene references, but longer than those of $Fe(C_{60}Me_5)Cp$ and $Fe(C_{60}Ph_5)Cp$. Surprisingly, the differential absorptions of the bucky ruthenocenes, taken at the conclusion of the singlet decay (i.e., 300 ps), are identical with those of the fullerene triplets, despite the inherently faster deactivation. A possible rationale for the faster deactivation is a heavy atom effect due to Ru, which accelerates the spin-forbidden intersystem crossing, thus dictating the reactivity of photoexcited $Ru(C_{60}Me_5)Cp$ and $Ru(C_{60}Ph_5)Cp$.

Nanosecond spectra further substantiated the notion of an accelerated intersystem crossing. The fullerene triplets are formed in 93 ± 3% yields, relative to the corresponding references (i.e., $C_{60}Me_5H$ and $C_{60}Ph_5H$) at identical absorption at the excitation wavelength. Interesting also is that the triplet lifetimes are around 1.5 μs, indicating that the heavy atom effect accelerates both spin-forbidden processes (i.e., singlet excited state → triplet excited state and triplet excited state → singlet ground state). An illustration of the fast triplet decay is given in Figure 9.

Additional pulse radiolytic oxidation experiments with $Ru(Cp)_2$ in aerated dichloromethane helped us to evaluate the spectral changes seen for $Ru(C_{60}Me_5)Cp$ and $Ru(C_{60}Ph_5)Cp$ (see Experimental Section for details). Figure S4 gathers the differential absorption changes following the $^{\bullet}OOCH_2Cl$- or $^{\bullet}OOCHCl_2$-induced oxidation of $Ru(Cp)_2$. The broad transition between 300 and 600 nm (features of the $[Ru(Cp)_2]^{\bullet+}$) are clearly different from the features seen on the femto-, pico-, nano-, and microsecond time scales of photoexcited $Ru(C_{60}Me_5)Cp$ and/or $Ru(C_{60}Ph_5)Cp$. Thus, the reaction sequence is summarized as follows:

$$Ru(C_{60}R_5)Cp \xrightarrow{h\nu} Ru(^1{}^*C_{60}R_5)Cp \xrightarrow{ISC} Ru(C_{60}R_5)Cp \quad (3)$$

In the final step of our photophysical investigation we analyzed the thermodynamic driving-force dependence on the rate constants, by applying eq 4, in which V represents the electronic coupling matrix element.[15]

$$k_{ET} = \left(\frac{4\pi^3}{h^2\lambda k_B T}\right)^{1/2} V^2 \exp\left[-\frac{(\Delta G^\circ_{ET} + \lambda)^2}{4\lambda k_B T}\right] \quad (4)$$

For our current analysis we transferred eq 4 to a linear expression (i.e., eq 5).

$$k_B T \ln k_{ET} + \frac{\Delta G^\circ_{ET}}{2} = k_B T \ln\left[\left(\frac{4\pi^3}{h^2\lambda k_B T}\right)^{1/2} V^2\right] - \frac{\lambda}{4} - \frac{(\Delta G^\circ_{ET})^2}{4\lambda} \quad (5)$$

The driving forces ($-\Delta G^\circ_{ET}$) were determined, on the basis of the first oxidation potential of the ferrocene donor and the

(18) Faraggi, M.; Weinraub, D.; Broitman, F.; DeFelippis, M. R.; Klapper, M. H. *Radiat. Phys. Chem.* **1988**, *32*, 293.
(19) (a) Guldi, D. M.; Hungerbühler, H.; Janata, E.; Asmus, K.-D. *J. Phys. Chem.* **1993**, *97*, 11258. (b) Guldi, D. M. *J. Phys. Chem. B* **2000**, *104*, 1483.

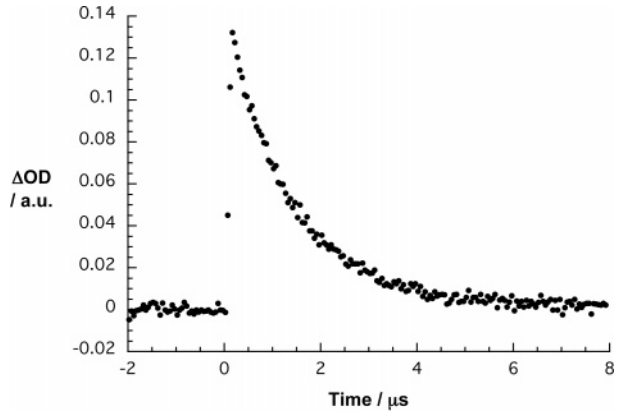

Figure 9. Time−absorption profiles of the Ru($C_{60}Me_5$)Cp triplet spectrum shown in Figure 6 at 660 nm, monitoring the decay of the fullerene triplet excited state.

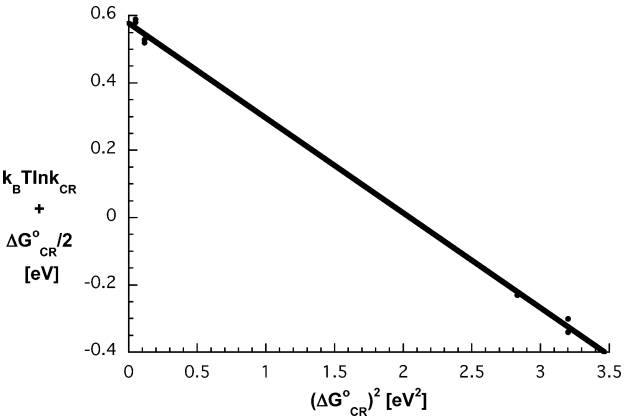

Figure 10. Plot of $[k_BT \ln k_{ET} + (\Delta G°_{ET}/2)]$ versus $(\Delta G°_{ET})^2$ for Fe(C_{60}-Me_5)Cp and Fe($C_{60}Ph_5$)Cp. The data include the charge separation and charge recombination values, see Table 1.

first reduction potential of the fullerene acceptors in toluene and THF, together with the energy level of the fullerene singlet excited state. In line with eq 5, plots of $[k_BT \ln k_{ET} + (\Delta G°_{ET}/2)]$ versus $(\Delta G°_{ET})^2$ give a linear correlation (see Figure 10). The reorganization energies (λ) and electronic coupling (V) values are obtained as 0.86 eV and 450 cm^{-1}, respectively. At first glance, the reorganization energy appears larger than those found in fullerene-porphyrin conjugates with values as small as 0.59 eV, but the notable charge density shifts and small orbital overlaps render such higher values inevitable.

The peculiar characteristics of the bucky ferrocene and ruthenocene as compared to their all-organic kin suggest that one can develop a new type of photovoltaic material on the basis of these organometallics. Among numerous elaborately designed donor-acceptor organofullerene compounds, the bucky ferrocene is unique for its symmetry and for the mechanism of π-conjugation. In addition, it has a potential of electronic tuning of the π-system by modification of substituents on the fullerene core and on the cyclopentadienide group. Our very recent discovery of synthetic routes to "double-decker" bucky ferrocene[22] (an additional ferrocene unit installed on the bottom of the fullerene core) suggests an even more fascinating possibility of the modulation of the conjugated system. Construction of photovoltaic systems based on bucky metallocenes will be the target in the forthcoming future.

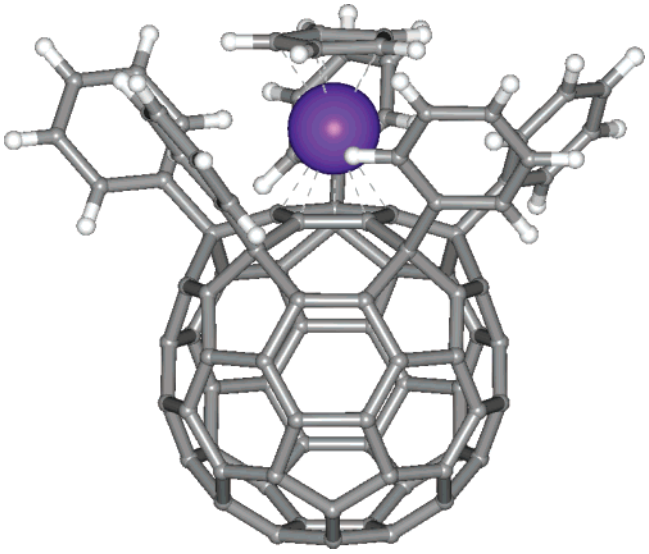

Figure 11. Crystal structure of Ru($C_{60}Ph_5$)Cp.

Conclusions

In conclusion, our work demonstrates that, despite realizing the shortest feasible donor-acceptor separation in a set of Fe($C_{60}R_5$)Cp [i.e., Fe($C_{60}Me_5$)Cp and Fe($C_{60}Ph_5$)Cp] and Ru($C_{60}R_5$)Cp [i.e., Ru($C_{60}Me_5$)Cp and Ru($C_{60}Ph_5$)Cp)] conjugates, all constituents (i.e., fullerene, ferrocene, and ruthenocene) largely preserve their chemical identity.[4,6−9,20,21] In this respect, photoexcitation of the fullerene leads to the population of the corresponding "localized" singlet excited states. In Fe($C_{60}R_5$)-Cp, extremely strong electronic couplings facilitate an excited-state electron-transfer deactivation that is prompt and quantitative. On the other hand, placing the weaker electron donor analogue of $Fe(Cp)_2$, namely, $Ru(Cp)_2$, within the same intimate contact (relative to the fullerene core) in Ru($C_{60}R_5$)Cp fails to cause notable electron-transfer interactions, both in the ground and excited states. Instead, intrinsically faster excited-state deactivations are confirmed as the only appreciable outcome.

Experimental Section

Synthesis of (η^5-Cyclopentadienyl)[(2,3,12,13,14-η^5)-1,4,11,15,30-pentaphenyl-1,2,4,11,15,30-hexahydro[60]fulleren-2-yl]ruthenium: Ru($C_{60}Ph_5$)Cp. All manipulations were performed under argon atmosphere using standard Schlenk techniques. High-pressure liquid chromatography (HPLC) was performed on Shimadzu HPLC system equipped with an Buckyprep column (Nacalai Tesque Co., 4.6 mm × 250 mm). Nuclear magnetic resonance (NMR) spectra were measured on a JEOL ECX-400 spectrometer. Mass spectra were acquired by

(20) (a) Guldi, D. M.; Marcaccio, M.; Paolucci, F.; Paolucci, D.; Ramey, J. *J. Phys. Chem. A* **2005**, *109*, 9723. (b) Araki, Y.; Yasumar, Y. Ito, O. *J. Phys. Chem. B* **2005**, *109*, 9843. (c) Guldi, D. M.; Imahori, H.; Tamaki, K.; Kashiwagi, Y.; Yamada, H.; Sakata, Y.; Fukuzumi, S. *J. Phys. Chem.* **2004**, *108*, 541. (d) Kanato, H.; Takimiya, K. Otsubo, T.; Aso, Y.; Nakamura, T.; Araki, Y.; Ito, O. *J. Org. Chem.* 2004, *69*, 7183. (e) D. Souza, F.; Smith, P. M. Gadde, S.; McCarty, A. L.; Kullman, M. J.; Zandler, M. E.; Itou, M.; Araki, Y.; Ito, O. *J. Phys. Chem. B* **2004**, *108*, 11333. (f) Imahori, H.; Sekiguchi, Y.; Kashiwagi, Y.; Sato, T.; Araki, Y.; Ito, O.; Yamada, H.; Fukuzumi, S. *Chem. Eur. J.* **2004,** *10*, 3184. (g) Fujitsuka, M.; Tsuboya, N.; Hamasaki, R.; Ito, M.; Onodera, S.; Ito, O.; Yamamoto, Y. *J. Phys. Chem. A* **2003**, *107*, 1452. (h) Langa, F.; de la Cruz, P.; Espildora, E.; Gonzales-Cortes, A.; de la Hoz, A.; Lopez-Arza, V. *J. Org. Chem.* **2000**, *65*, 8675. (i) Herranz, M. A.; Illescas, B.; Martin, N.; Luo, C.; Guldi, D. M. *J. Org. Chem.*, **2000**, 65, 5728. (j) Fujitsuka, M.; Ito, O.; Imahori, H.; Yamada, K.; Yamada, H.; Sakata, Y. *Chem. Lett.* **1999**, 721.

(21) Oviedo, J. J.; de la Cruz, P.; Garin, J.; Orduna, J.; Langa, F. *Tetrahedron Lett.* **2005**, *46*, 4781.

(22) Matsuo, Y.; Tahara, K.; Nakamura, E. *J. Am. Chem. Soc.* **2006**, *128*, 7154.

Table 2. Crystal Data and Data Collection Parameters of $Ru(C_{60}Ph_5)Cp\cdot 3CS_2$

formula	$C_{98}H_{30}Ru_1S_3$	V, Å^3	6234.9(5)
crystal system	monoclinic	Z	4
space group	$P2_1/n$ (No. 14)	T, K	120(2)
R, R_w ($I > 2\sigma(I)$)	0.0733, 0.2053	crystal size, mm	0.32, 0.24, 0.18
R1, wR2 (all data)	0.0815, 0.2137	D_{calcd}, g/cm^{-3}	1.599
GOF on F^2	1.031	$2\theta_{min}$, $2\theta_{max}$, deg	4.36, 51.14
a, Å	17.7250(9)	no. refl. measured (total)	11173
b, Å	14.0460(7)	no. refl. measured ($I > 2\sigma(I)$)	9685
c, Å	26.1310(7)	no. parameters	947
α, deg	90	Δ, eÅ^{-3}	1.45, −1.322
β, deg	106.589(3)	μ	0.512
γ, deg	90		

atmospheric pressure ionization (APCI) using quadrupole mass analyzer on Shimadzu QP-8000 spectrometer.

To a suspension of $C_{60}Ph_5H$ (1.00 g, 0.903 mmol) in THF (300 mL) was added a solution of KO^{t}Bu (1.0 M, 1.13 mL, 1.13 mmol) in THF. The reaction mixture was stirred for 20 min at 25 °C. To the resulting dark-brown solution, $[RuCp(CH_3CN)_3][PF_6]$ (588 mg, 1.35 mmol) was added in one portion. The suspension was stirred for 20 min, and then the solvent was removed in reduced pressure. The crude mixture was dissolved in toluene, and the solution was passed through a pad of silica gel. After preparative HPLC separation [Buckyprep (Nacalai Tesque Co., 20 mm × 250 mm), toluene/2-propanol = 1:1, flow rate = 20 mL/min, retention time = 8.0−9.0 min] and recrystallization from the mixture of CS_2/EtOH, Ru(η^5-$C_{60}Ph_5$)(η^5-C_5H_5) was obtained as air-stable, red crystals (689 mg, 0.542 mmol, 60% yield). ^{1}H NMR (400 MHz, $CDCl_3$): δ 3.52 (s, 5H), 7.16 (t, ^3J = 7.8 Hz, 10H), 7.26 (t, ^3J = 7.4 Hz, 5H), 7.66 (d, ^3J = 7.2 Hz, 10H). $^{13}C\{^1H\}$ NMR (100 MHz, $CDCl_3$): δ 58.42 (5C, *C*-Ph), 77.46 (5C, Cp), 99.72 (5C, FCp), 127.40 (10C, Ph), 127.46 (5C, Ph), 128.89 (10C, Ph), 143.22 (10C), 143.82 (10C, Ph), 144.26 (10C), 147.41 (5C), 148.14 (10C), 148.45 (5C), 152.47 (10C). IR (neat): ν(C−H)/cm^{-1} 2958 (m), 2925 (m), 2958 (m). APCI-MS(−): m/z = 1272 (M^-).

X-ray Crystallographic Analysis of Ru($C_{60}Ph_5$)Cp. Single crystals of Ru(η^5-$C_{60}Ph_5$)Cp suitable for an X-ray diffraction study were grown and subjected to data collection. The data set was collected on a MacScience DIP2030 imaging plate diffractometer using Mo Kα (graphite monochromated, λ = 0.71069 Å) radiation. Crystal structure and crystal data are shown in Figure 11 and Table 2. The structure of Ru(η^5-$C_{60}Ph_5$)Cp was solved by the direct method (SIR97).[23] The positional and thermal parameters of non-hydrogen atoms were refined anisotropically on F^2 by the full-matrix least-squares method, using SHELXL-97.[24] Hydrogen atoms were placed at calculated positions and refined with a riding mode on their corresponding carbon atoms. In the subsequent refinement, the function $(F_o^2 - F_c^2)^2$ was minimized, where $|F_o|$ and $|F_c|$ are the observed and calculated structure factor amplitudes, respectively. The agreement indices are defined as R1 = $|(|F_o| - |F_c|)|/\sum|F_o|$ and wR2 = $[\sum w(F_o^2 - F_c^2)^2/\sum (wF_o^4)]^{1/2}$.

Molecular orbital calculations were performed by the hybrid DFT method (B3LYP) with the GAUSSIAN 98 program package.[25] To obtain the molecular orbital (Kohn−Sham orbital), the molecular geometry including the carbon and iron atoms was fixed at an average crystallographic structure of bucky ferrocene (C_{5v}), and the positions of the hydrogen atoms were first optimized under C_{5v} symmetry using the Ahlrichs-TZV all-electron basis set for the Fe atom and the 6-31G-(d) basis set for the C and H atoms.[26]

Femtosecond transient absorption studies were performed with 387-nm laser pulses (1 kHz, 150-fs pulse width) from an amplified Ti: Sapphire laser system (Clark-MXR, Inc.). Nanosecond laser flash photolysis experiments were performed with 337-nm laser pulses from a nitrogen laser (8-ns pulse width) in a front face excitation geometry. Fluorescence lifetimes were measured with a Laser Strobe fluorescence lifetime spectrometer (Photon Technology International) with 337-nm laser pulses from a nitrogen laser fiber coupled to a lens-based T-formal sample compartment equipped with a stroboscopic detector. Details of the Laser Strobe systems are described on the manufacture's web site. Emission spectra were recorded with a SLM 8100 spectrofluorometer. The experiments were performed at room temperature. Each spectrum represents an average of at least five individual scans, and appropriate corrections were applied whenever necessary.

Pulse radiolysis experiments were performed using 50-ns pulses of 15 MeV electrons from a linear electron accelerator (LINAC). Dosimetry was based on the oxidation of SCN^- to $(SCN)_2^{\bullet -}$ which in aqueous, N_2O-saturated solution takes place with $G \approx 6$ (G denotes the number of species per 100 eV, or the approximate μM concentration per 10 J absorbed energy). The radical concentration generated per pulse was varied between $(1-3) \times 10^{-6}$ M. The reductive electron-transfer reactions were studied by radiation-induced reduction in N_2-saturated toluene/2-propanol/acetone (8:1:1 v/v/v).[27] The reducing species, generated under these conditions, are $(CH_3)_2{}^{\bullet}C(OH)$ radicals, i.e., the radicals formed by hydrogen abstraction from 2-propanol and from electron capture of acetone followed by a subsequent protonation. The oxidative electron-transfer studies were carried out in oxygenated dichloromethane. Upon radiolysis, the generation of the short-lived, strongly oxidizing solvent radical cation ($[CH_2Cl_2]^{\bullet +}$) takes place.[28] The radiolysis of dichloromethane also leads to the carbon centered $^{\bullet}CH_2Cl$ and $^{\bullet}CHCl_2$ radicals, particularly in the absence of a radical cation scavenger. These are formed via dissociative electron capture and proton loss, respectively. In oxygenated solvents the radical formation is followed by a rapid reaction with molecular oxygen, yielding the respective oxidizing $^{\bullet}OOCH_2Cl$ and $^{\bullet}OOCHCl_2$ peroxyl radicals. It is important to note that $[CH_2Cl_2]^{\bullet +}$ itself does not react with molecular oxygen.

Acknowledgment. This work was supported by EU (RTN network "WONDERFULL"), SFB 583, DFG (GU 517/4-1), FCI, and the Office of Basic Energy Sciences (NDRL 4672) of the U.S. Department of Energy and 21st Century COE Program for Frontiers in Fundamental Chemistry. We thank Jeff Ramey for performing some preliminary measurements.

Supporting Information Available: Complete ref 25; time-resolved fluorescence profiles; plot of k_{obs} vs $[O_2]$; time-absorption profiles; differential absorption spectrum. This material is available free of charge via the Internet at http://pubs.acs.org.

JA061120V

(23) Altomare, A.; Burla, M. C.; Camalli, M.; Cascarano, G. L.; Giacovazzo, C.; Guagliardi, A.; Moliterni, A. G. G.; Polidori, G.; Spagna, R. *J. Appl. Crystallogr.* **1999**, *32*, 115.
(24) Sheldrick, G. M. *Programs for Crystal Structure Analysis*, Release 97-2; Institut für Anorganische Chemie der Universität: Götingen, Germany, 1998.
(25) Frisch, M. J.; et al. *Gaussian 98*, Revision A.6; Gaussian Inc.: Pittsburgh PA, 1998.
(26) Schafer, A.; Horn, H.; Ahlrichs, R. *J. Chem. Phys.* **1992**, *97*, 2571.
(27) Guldi, D. M.; Hungerbühler, H.; Janata, E.; Asmus, K.-D. *J. Phys. Chem.* **1993**, *97*, 11258.
(28) Shank, N. E.; Dorfman, L. M. *J. Chem. Phys.* **1970**, *52*, 4441.